

Synthesis and characterization of magnetite nano particles with high selectivity using in-situ precipitation method

Citation for published version (APA):

Rashid, H., Mansoor, M. A., Haider, B., Nasir, R., Abd Hamid, S. B., & Abdulrahman, A. (2020). Synthesis and characterization of magnetite nano particles with high selectivity using in-situ precipitation method. *Separation Science and Technology*, 55(6), 1207-1215. <https://doi.org/10.1080/01496395.2019.1585876>

DOI:

[10.1080/01496395.2019.1585876](https://doi.org/10.1080/01496395.2019.1585876)

Document status and date:

Published: 12/04/2020

Document Version:

Publisher's PDF, also known as Version of Record (includes final page, issue and volume numbers)

Please check the document version of this publication:

- A submitted manuscript is the version of the article upon submission and before peer-review. There can be important differences between the submitted version and the official published version of record. People interested in the research are advised to contact the author for the final version of the publication, or visit the DOI to the publisher's website.
- The final author version and the galley proof are versions of the publication after peer review.
- The final published version features the final layout of the paper including the volume, issue and page numbers.

[Link to publication](#)

General rights

Copyright and moral rights for the publications made accessible in the public portal are retained by the authors and/or other copyright owners and it is a condition of accessing publications that users recognise and abide by the legal requirements associated with these rights.

- Users may download and print one copy of any publication from the public portal for the purpose of private study or research.
- You may not further distribute the material or use it for any profit-making activity or commercial gain
- You may freely distribute the URL identifying the publication in the public portal.

If the publication is distributed under the terms of Article 25fa of the Dutch Copyright Act, indicated by the "Taverne" license above, please follow below link for the End User Agreement:

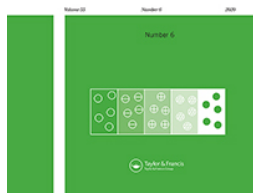
www.tue.nl/taverne

Take down policy

If you believe that this document breaches copyright please contact us at:

openaccess@tue.nl

providing details and we will investigate your claim.



ISSN: 0149-6395 (Print) 1520-5754 (Online) Journal homepage: <https://www.tandfonline.com/loi/lst20>

Synthesis and characterization of magnetite nano particles with high selectivity using in-situ precipitation method

Harith Rashid, Muhammad Adil Mansoor, Bilal Haider, Rizwan Nasir, Sharifah Bee Abd Hamid & Aymn Abdulrahman

To cite this article: Harith Rashid, Muhammad Adil Mansoor, Bilal Haider, Rizwan Nasir, Sharifah Bee Abd Hamid & Aymn Abdulrahman (2020) Synthesis and characterization of magnetite nano particles with high selectivity using in-situ precipitation method, Separation Science and Technology, 55:6, 1207-1215, DOI: [10.1080/01496395.2019.1585876](https://doi.org/10.1080/01496395.2019.1585876)

To link to this article: <https://doi.org/10.1080/01496395.2019.1585876>



© 2019 The Author(s). Published with license by Taylor & Francis Group, LLC.



Published online: 08 Mar 2019.



Submit your article to this journal [↗](#)



Article views: 1787



View related articles [↗](#)




View Crossmark data [↗](#)



Citing articles: 4 View citing articles [↗](#)

Synthesis and characterization of magnetite nano particles with high selectivity using in-situ precipitation method

Harith Rashid^{a,b}, Muhammad Adil Mansoor^c, Bilal Haider^d, Rizwan Nasir ^e, Sharifah Bee Abd Hamid^a, and Aymn Abdulrahman^e

^aNanotechnology & Catalysis Research Centre (NANOCAT), University of Malaya, Kuala Lumpur, Malaysia; ^bDepartment of Chemical Engineering & Chemistry, Eindhoven University of Technology, Eindhoven, the Netherlands; ^cDepartment of Chemistry, School of Natural Sciences (SNS), National University of Science and Technology, (NUST), Islamabad, Pakistan; ^dChemical Engineering, Institute of Chemical Engineering and Technology (ICET), University of the Punjab, Lahore, Pakistan; ^eFaculty of Engineering, Department of Chemical Engineering, University of Jeddah, Jeddah, Saudi Arabia

ABSTRACT

In-situ precipitation method is widely used and reported in the literature for the synthesis of iron oxide nanoparticles based on their applications in many fields. However, the rate of reaction and rate constant for the production of Magnetite Phase of iron oxide did not study in depth. Reaction rates are required to design a scale-up of the process. In this study, Magnetite phase of iron oxide nanoparticles (Fe_3O_4) are synthesized by the in-situ precipitation method, and the overall reaction rate is evaluated based on the concentration of Magnetite produced during the process. Further, X-ray diffraction, energy-dispersive X-ray spectroscopy and Raman spectroscopy are used to confirm the presence of a higher proportion of magnetite (Fe_3O_4) in the final product, which is responsible for more top magnetic properties 74.615 emu. Changes in morphology of these nanoparticles at different intervals of the reaction are reported by transmission electron microscope. The results showed that spherical nanoparticles synthesized at different intervals of the reaction have a very narrow range of particle size, i.e. 9–15 nm. Detailed analysis reveals the presence of a higher share of maghemite (Fe_2O_3) at the start of the reaction. However, maghemite eventually is converted to magnetite by the end of the reaction, thereby enhancing the magnetic strength of the nanoparticles.

ARTICLE HISTORY

Received 3 May 2018
Accepted 19 February 2019

KEYWORDS



Magnetite; coprecipitation; super para-magnetic; agglomeration; break-up

Introduction

There are about 16 different phases of iron oxide reported to date.^[1] All of these iron oxide phases are crystalline except two, schwertmannite, and ferrihydrite.^[2] Production of metallic nanoparticles and using them for their superparamagnetic properties are quite common in therapeutic and diagnostic applications, such as magnetic resonance imaging (MRI).^[3,4] These iron oxides find applications as catalysts,^[5] sorbents,^[6] pigments,^[7] flocculants,^[8] coatings,^[9] gas sensors,^[10,11] wastewater treatment,^[12] and for lubrication.^[13,14] Similarly these nano particles can also be used in different advanced processes to form nano reactor, added into polymer films and other products, based on their superior magnetic properties.^[15] These applications make magnetite super magnetic nanoparticles of iron oxide, and there is a need for development and modification of such synthesis processes with least operational cost.

Based on the magnetic properties of iron oxide crystals, three main phases are well known for their higher magnetic strength with magnetite being on top of the list followed by maghemite and hematite.^[1] There are several different methods for production of iron oxide nanoparticles such as coprecipitation,^[16] sol-gel,^[17] hydrothermal,^[18] emulsion-precipitation,^[19] micro-emulsion^[20] and microwave assisted hydrothermal technique.^[21] However, the focus is on having a magnetite phase of iron oxide with high purity. In this case, the solid phase is produced by neutralization reaction and rapid mixing, which is crucial for controlling grain size and magnetic properties.

Precipitation and surface morphology is the result of several mechanisms, namely, nucleation, molecular growth and secondary processes such as aggregation/coalescence and breakage of particles and the driving force for production of nanoparticles is supersaturation. Nucleation is the first step for formation of

CONTACT Harith Rashid  harith.rashid.raza@gmail.com  Reactor Engineering Lab, Department of Chemical Engineering and Chemistry, Eindhoven University of Technology, Eindhoven, the Netherlands.

Color versions of one or more of the figures in the article can be found online at www.tandfonline.com/lsst.

© 2019 The Author(s). Published with license by Taylor & Francis Group, LLC.

This is an Open Access article distributed under the terms of the Creative Commons Attribution-NonCommercial-NoDerivatives License (<http://creativecommons.org/licenses/by-nc-nd/4.0/>), which permits non-commercial re-use, distribution, and reproduction in any medium, provided the original work is properly cited, and is not altered, transformed, or built upon in any way.

nanoparticles and occurs when the critical number of molecules join together to form an embryo. Stable embryos from nuclei act as a seed in the solution for precipitation of other molecules.^[22] Aggregation and growth result in attaching two particles and growth of these nanoparticles, respectively. The aggregate characterized by slow rates and occur after particles formation and depends on the force with which two particles collide. Most of the collisions do not have enough energy to agglomerate the particles and particles bounce back into the system.^[23] Most of the metal oxide nanoparticles also have a surface charge, and the strength of these surface charges also reduce the chance of aggregation or coalescences of particles.^[24]

Break-up of particles depends on different forces acting on the particles during its motion in the fluid. Particles with sharp edges and uneven surface have more chance of breaking into two or more than two smaller particles, depending on the forces balance on particles.^[25] However, this phenomenon is very rare in metal oxide nanoparticles. Mechanical forces in the metallic oxides are very high as compared to surface forces acting on the particles and it can be assumed zero in case of nanoparticles.^[26]

Precipitation of iron salts with the strong basic solution in a turbulent mixing regime generated super saturation and caused transport of freshly formed particles into regions with super high saturation. In high mixing regimes, small particles produced by high nucleation rates and growth of these nanoparticles are dependent on mixing efficiency. Since the precipitation reactions are very fast, the effect of mixing is significant down to micro-mixing level. This phenomenon is more prominent at high mixing rates and will depend on the flow regime in the reactor.^[25]

This study is focused on producing magnetite nanoparticles by coprecipitation process. One of the major contributions in the present work is to report change in magnetite concentration with reaction time. Coprecipitation reactions between iron salts and precipitating agent are very fast resulting in different products formed as soon as first drop is mixed into the solution. However, Magnetite formation is based on a slow reaction and required relatively large reaction time. Selectivity of Magnetite production in the solution is quite sensitive and depends on operating parameters such as pH, reaction temperature, concentration and iron salt molar ratio.^[27] Thus, the objective of this work is to synthesize super paramagnetic iron oxide nanoparticles, i.e. magnetite (Fe_3O_4) with high purity. Initially, the experimental set-up and process of coprecipitation is described. Then nanoparticles are characterized for concentration of different crystals in the product and finally the size and magnetic strength of these nanoparticles are reported.

Experimental procedure

Ferrous chloride tetrahydrate ($\text{FeCl}_2 \cdot 4\text{H}_2\text{O}$) was supplied by R&M chemicals® with 99% purity, ferric chloride hexahydrate ($\text{FeCl}_3 \cdot 6\text{H}_2\text{O}$) and ammonia solution (28% NH_4OH), were supplied by from Merck®. These salts and solvents were used without further purification.

In a typical reaction 100 mL of deionized (DI) water was added in to a 2200 mL conical glass vessel (reactor) equipped with four axial blade propellers with a 2" pitch. Reynolds number for the propeller was calculated from equation for Reynold's number of an impeller defined as in Equation 1:

$$Re = (\rho n D^2) / \mu \quad (1)$$

The power number for impellers of all sizes can be calculated from equation 2 given below:

$$Np = P_{imp} / (\rho n^3 D^5) \quad (2)$$

where P_{imp} is the amount of power transferred from the impeller to the fluid. Transitional regime between laminar and turbulent regime exists when the Reynolds number of the reactor is more than the Reynolds number describing the transition from laminar to turbulent flow in Equation 3:

$$Re_{TT} = 6.370 Np^{-1/3} \quad (3)$$

For experimental purposes, the reactor was initially filled with a small quantity of DI water and was stirred at 500 rpms and 60°C. The iron precursor solution was prepared by mixing 21.2 g (0.106 mol) $\text{FeCl}_2 \cdot 4\text{H}_2\text{O}$ and 57.42 g (0.212 mol) $\text{FeCl}_3 \cdot 6\text{H}_2\text{O}$ into DI water and temperature of the system was maintained at 60°C. Neutralization reaction starts as soon as the freshly prepared 1 L solution of 9 M NH_4OH was added gradually into the reactor at a flow rate of 100 mL/min. The volume of the reactor at this time was 2 L and reaction was carried out at the transition between laminar and turbulent regime. All the openings of the reactor were closed carefully, and the reaction mixture was agitated vigorously at 500 rpm, for 90 min.

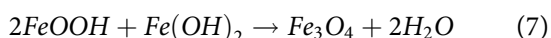
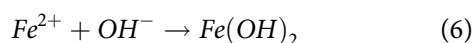
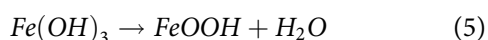
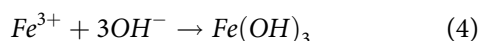
Dimensionless mixing time for the reactor is defined as the product of mixing time for the reactor and propeller speed (units of time^{-1}). This value is not dependent on the fluid regime and depends on power dissipation and selectivity of the reactor in case of turbulent flows. Details of mixing time will be discussed based on the selectivity of production of magnetite.

Samples were collected at different time intervals and were placed on permanent magnetic pads, to hasten sedimentation of magnetic nanoparticles. The solution from the top was decanted, and the nanoparticles

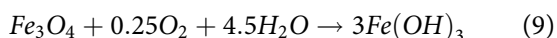
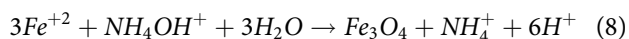
were washed with DI water until pH reduces to 8. This step ensured that the completion of the reaction and the nanoparticles were extracted for characterization purpose.

Reaction mechanism

The reaction between iron precursor solution and the precipitating agent is slightly exothermic. The formation of iron oxide nanoparticles starts as soon as ammonium hydroxide is added into iron salts and the mechanism for this process has been reported in the literature.^[28] Reaction for formation of iron oxide nanoparticles is shown in chemical Equation 4–7.^[16]



All of these reactions are pseudo instantaneous making it difficult to predict the behavior of the reactor. The reaction for production of magnetite is relatively slower than other neutralization reactions, and therefore a very low concentration of magnetite is expected to be present at the start of the reaction. However, oxidation of iron oxide crystals to magnetite is one of the primary sources for increasing the concentration of magnetite in the end product as shown by equation 8. Oxidation of magnetite to ferric hydroxide is more prominent at higher pH resulting in formation of intermediate product and more energy consumption.^[29] Therefore, the reaction mixture is mixed in high pH range and is mixed for a longer time to increase the selectivity of the process toward magnetite. The reaction is done at atmospheric temperature, and all the opening of the reactor was sealed to avoid the entrance of oxygen into the reactor. The oxygen can limit the transformation of magnetite to other phases, i.e. maghemite and goethite and some time to hematite.^[30] Another side reaction that takes place in presence of oxygen is oxidation of Fe (II) and Fe (III).^[31]



Because of the factors as mentioned above, the parameters effecting rate of reaction were modified and controlled to increase the production of magnetite nanoparticles. Formation of impurities is standard practice of any chemical reaction, thus specially designed external magnetic pads at the bottom of the beaker were used to eliminate the impurities while the effluent was drained from the top of the beaker.

Reaction rate

The reaction between iron (II), Iron (III) chlorides and ammonium hydroxide is heterogeneous. The rate of production of Iron oxide nanoparticles is shown in Table 1. It can be observed that the weight of nanoparticles production increases with time. The temperature of the reactor was sustained at 60°C. It can be seen that there is a higher production rate, i.e. faster reaction rate at the start of the reaction, but it decreases gradually during the reaction. It is also important to note that different phases of iron oxide can be present in the product as discussed earlier. As it is a neutralization reaction and depends on the concentration of iron salts, the rate of nanoparticle production decreases as time increases. It is based on the fact that as the time lapse, most of the iron salts are converted into nanoparticles.

Overall rate of reaction equation can be modified based on the data available in the reaction between iron (II), Iron (III) chlorides and ammonium hydroxide is heterogeneous. The rate of production of Iron oxide nanoparticles is shown in Table 1. It can be observed that the weight of nanoparticles production increases with time. The temperature of the reactor was sustained at 60°C. It can be seen that there is a higher production rate, i.e. faster reaction rate at the start of the reaction, but it decreases gradually during the reaction. It is also important to note that different phases of iron oxide can be present in the product as discussed earlier. As it is a neutralization reaction and depends on the concentration of iron salts, the rate of nanoparticle production decreases as time increases. It is based on the fact that as the time lapse, most of the iron salts are converted into nanoparticles.

$$r = 2.074 \times 10^{-4} [\text{FeCl}_2][\text{FeCl}_3]^2 \quad (10)$$

Table 1. Weight of iron oxide nanoparticles with respect to time.

Time (min)	Weight of nanoparticles gm	pH of liquid	percentage Magnetite (XRD) %	Magnetite (10 ³) gm/m ³	Reaction rate (10 ³) gm/m ³ .min
20	2.164	10.25	4.8	2.5968	0.12984
40	3.178	10.05	15.3	12.15585	0.303896
60	3.295	10	35.6	29.3255	0.488758
80	3.403	9.8	90.3	76.82273	0.960284
90	3.444	9.8	98.2	84.5502	0.939447

Characterization

The X-ray diffraction (XRD) patterns for all the samples based on their crystal structure of the nanoparticles are recorded using Cu K α radiation on a Rigaku Ru2000 rotating anode diffractometer. The FTIR spectra were obtained using a Perkin-Elmer 100 spectrophotometer (Waltham, MA, USA) over the range of 400–3000 cm⁻¹ under standard operating conditions. The structural properties are also investigated using a Raman microscope, Renishaw (Gloucestershire, UK), in the range of 100–2000 cm⁻¹. Magnetization saturation for all the samples are reported as a full magnetization curve of nanoparticles, examined using a vibrating sample magnetometer (VSM 880, DMS/ADE Technologies, USA). Zeta potential and particle size are measured using a Zetasizer Nano ZS apparatus. The Zeta potential and hydrodynamic diameter of nanoparticles is measured by dispersing 0.005 g of dried nanoparticles in 10 mL distilled water.

Results and discussion

X-ray diffraction

The XRD pattern of synthesized nanoparticles of iron oxide is very matched with JCPDS card [19-0629] for magnetite. The reflection at 2 θ values of 30°, 35°, 43°, 57°, and 63° corresponds to lattice planes of (220), (311), (400), (422), (511), and (440), respectively for magnetite. Furthermore, the Scherer's equations with a pseudo-Voigt Function^[16,32] was applied on the peak at 2 θ of 35° to attain the crystallite size of iron oxide nanoparticles, extracted at different time intervals.

As the process is based on neutralization reactions, which have high reaction rates and all the reactants are soluble in water with no mass transfer limitation. Similarly, the solubility of the iron oxides formed is almost zero in water. Therefore, the bulk solution is supersaturated as soon as a precipitating agent is dropped into the reactor.

Iron oxide produced instantaneously after addition of initial drops of precipitating agent supersaturate the bulk solution and are responsible for the production of initial seeds of iron oxide crystals. The number of these seed increase with time until they are homogenized in the bulk solution to promote nucleation and growth of the crystals. Bulk solution is considered to be supersaturated with iron oxide until all the precipitating agent is added. As iron oxide is continuously transferred out from the bulk liquid, the viscosity of the solution continues to increase, until all the iron oxide is transferred out of the liquid phase.

Selectivity

Selectivity of magnetite nanoparticle production is dependent on micro-mixing efficiency and energy dissipation of the mixer. Neutralization reaction for maghemite is pseudo instantaneous as the product is very stable, which is also evident from an initial 95.5 wt. % of maghemite and 4.8 wt. % for magnetite at 20 min to reaction (Fig. 1). However, with time the concentration of magnetite increases and reaches at 90.3% at the elapsed time of 80 min and finally becomes 98.2% at the end of the reaction (90 min). This phase transfer is based on relatively slow oxidation of maghemite at higher pH of the solution.

Magnetic properties

Magnetic properties of solids are characterized by magnetic susceptibility, the permeability and magnetic moment. These properties are more prominent when metal oxide crystals placed in a magnetic field.^[33] Magnetic susceptibility (κ) is defined as a function of magnetic field strength, H and magnetization intensity, J as shown in Equation 11.

$$J = H \cdot \kappa \quad (11)$$

Magnetic permeability, μ , can be defined as the tendency of the magnetic lines of force to go through any medium (crystals) relative to their tendency to pass through a perfect vacuum.^[34] This parameter is calculated from the equation given below:

$$\mu = \mu_0(1 + k) \quad (12)$$

This helps in classifying different catalysts as diamagnetic and paramagnetic materials. Magnetic flux, density of magnetic lines of forces in a solid located in a magnetic field (H) is calculated from magnetic induction (B), Using the equation given below:

$$B = \mu(H + J) \quad (13)$$

Magnetic moment (m) of a crystal is also an important parameter to quantify the magnetic properties of a crystal (material). It is calculated from the measured molar susceptibility using the correlation given in Equation 14

$$\varphi = \mu_0 \frac{Nm^2}{3kT} \quad (14)$$

where N is Avogadro number and k is Boltzmann constant for materials. Bohr magneton (β) is fundamental magnetic moment and is calculated from Equation 15. Bohr magneton has a constant value of 9.2734×10^{-24} .

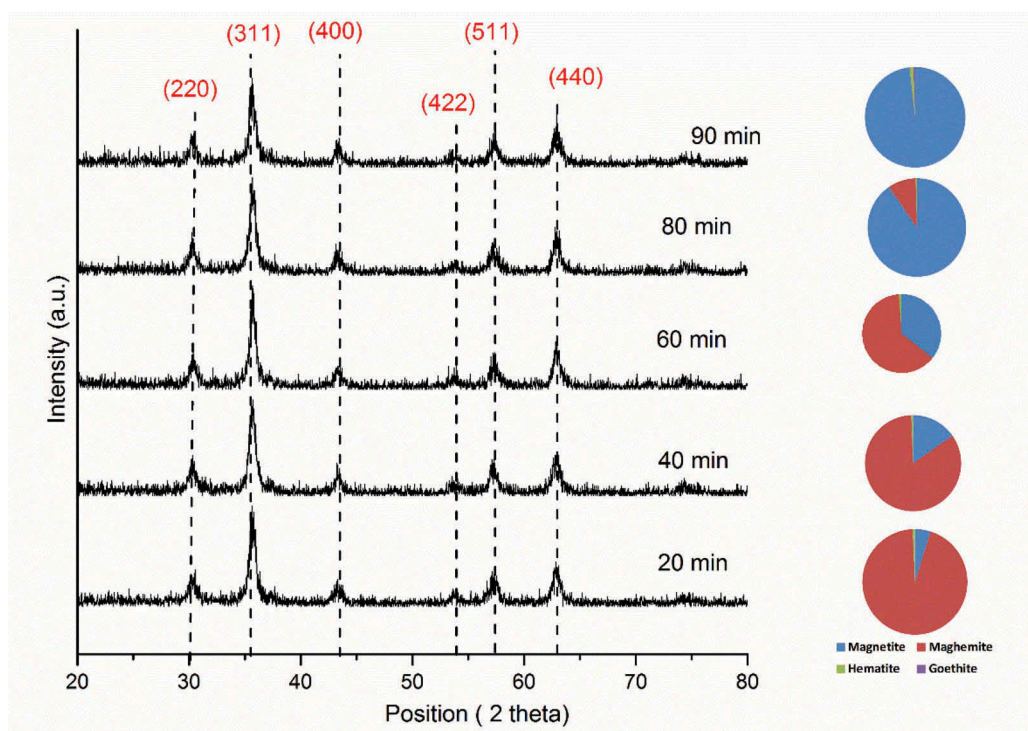


Figure 1. XRD analysis of iron oxide nano particles with different peaks.

$$\beta = \frac{eh}{4\pi m_e c} \quad (15)$$

The magnetic moment (μ_s) occurs due to the spin moment of the electron and has a units of Bohr magnetons.

where m_e in equation 15 is mass of the electron and e represents the electron charge. Bohr magneton has a constant value of 9.2734×10^{-24} .

Magnetization saturation (M_s), Coercivity (H_c), and remanence (M_r) of iron oxide nanoparticles for samples collected at different time intervals of the reaction are shown in Fig. 2. In the beginning, when the concentration of maghemite was higher, the magnetic strength of nanoparticles recorded was 66.651 emu. While the strength of these particles improved with the passage of time and reached the value of 71.332 at the elapsed time of 80 min. We believe this rise in magnetic strength is due to the formation of the magnetite phase of iron oxide. Furthermore, at the completion of reaction (90 min) the magnetic strength increases to 74.615 emu. Magnetization curves for all the samples are shown in Fig. 2. All the samples show same trend with very little deviation at the origin.

Iron oxide is known for its magnetite and paramagnetic properties. Randomly aligned, unpaired electrons in iron oxide crystals are captivated in the presence of an electrical or magnetic field.^[35]

Magnetic behavior of these crystals is temperature dependent and is expressed by the Curie–Weiss Law as shown in Equation 16.

$$\varphi_m = \frac{C_M}{T - T_C} \quad (16)$$

where C_M is Curie constant, T is operating temperature and, T_C is Curie temperature for the nanoparticles. Increase in the temperature may result in thermal vibration and thereby reducing the alignment of unpaired electron pairs, resulting in a reduction in overall value for magnetic strength φ_m . Coercivity and remanence for all the samples remain in the low range, and for the final product, the values are 19.940 and $-2.185/2.399$, respectively. It is reported that the magnetic behavior of iron oxide nanoparticles enhances with the decrease in particle size.^[36]

Surface charge analysis

One of the interesting property of metal oxides is their ability to have a surface charge, which enables these particles to be used in different applications.^[37] Therefore, Zeta potential of nanoparticles is measured for all the samples, and it is relatively high (-29.6 mV) from the start of the reaction and increases with time as shown in Table 2, and indicates that with an increase of magnetite concentration in the particles, surface charge of the nanoparticles increases from -29.6 to -41.8 mV.

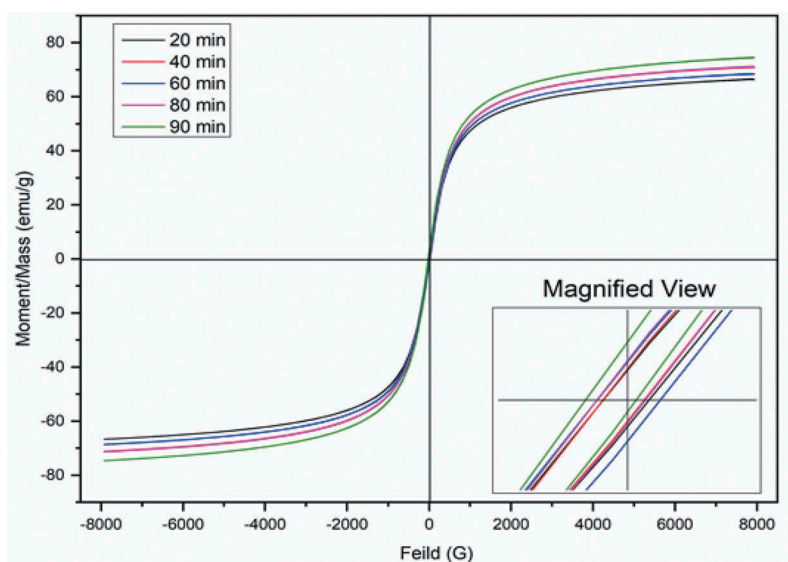


Figure 2. Magnetization curve for nanoparticles at different intervals.

Table 2. Zeta potential of magnetite nanoparticles at different reaction times.

Time (mins)	Zeta Potential (mV)
20	-29.6
40	-24.5
60	-24.3
80	-38.2
90	-41.8

Coalesces

Surface charge can be one of the reasons behind the small size of nanoparticles produced in this process.^[38] Although one of the significant advantages of high surface charge is the ability of nanoparticles to make stable suspensions it also identifies that the chance of coalesces of nanoparticles is low.^[25,39] The energy required for aggregation (coalesces) is a much higher and negative surface charge on the particles is also very high and more energy is needed to overcome charge density on both of the particles colliding with each other.^[40] As the reactor used in this research is conical in shape, and the flow is moving in only one direction. Therefore, the chance of collision of two particles with that high forces to attach can be assumed to be zero, and all the particles will move back into the bulk solution after the collision. The collision of nanoparticles with the wall of the reactor and with the propeller can be neglected in this process as those nanoparticles remain attached to the walls of the reactor and are not part of the product.

Break-up

The break-up of nanoparticles can always be a part of the process for particles with high particle size.^[25]

Break-up based on force balance on the surface of the particle is assumed to be zero as it is impossible for the mixing regime to overcome mechanical bondage between the particles. However, the collision of nanoparticles with the propeller and walls of the reactor play a significant role in breaking the particles into smaller pieces. Based on the centripetal force, particles will move toward the walls of the reactor to collide with the wall of the reactor. The collision of particles with relatively larger sizes will have significant impact on the collision with the wall resulting in cracks in the particles which can lead to break up.

Surface morphology

Shape and size of the nanoparticles produced in this research are discussed in details in this section. TEM images of iron oxide nanoparticles extracted at different reaction times of 20, 60, and 90 min are shown in Fig. 3(a-c). Crystal scattering for these samples is shown in Fig. 3 (d-f, respectively). Size of the nanoparticles produced in this research is in the range of 9–15 nm. The process of nanoparticles production used in this research is quite complex based on its reaction and mixing regimes. Reaction and production of iron oxide nanoparticles depend on the selectivity of the different reactions at the starting phase of the process. However, later part of the process is dominated by mixing behaviors of the process with a very slow reaction for phase change of maghemite to magnetite. It can be seen from Fig. 3(a) that the shape of most of the nanoparticles is spherical with exceptions of small edges attached to some nanoparticles.

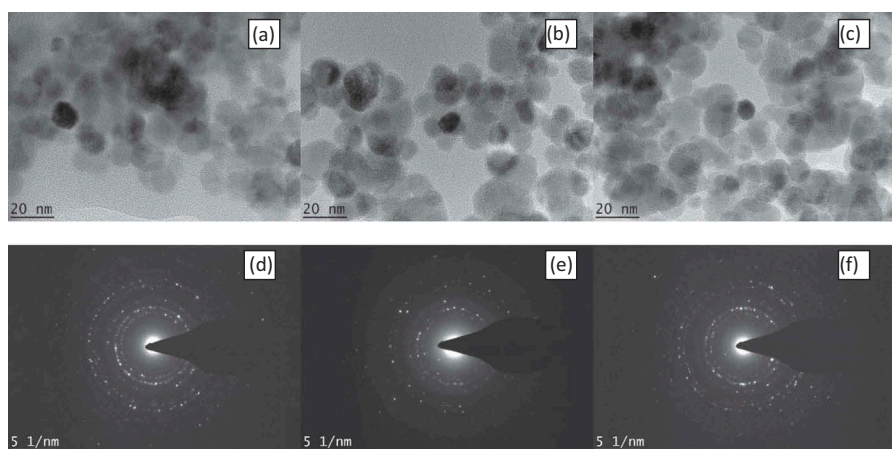


Figure 3. TEM images for iron oxide nanoparticles at (a) 20 min, (b) 60 min and (c) 90 min and crystal scattering for samples taken at (d) 20 min, (e) 60 min, (f) 90 min.

As mentioned in the earlier section, different phenomena are prominent in the solution which results in the smaller size of the nanoparticles. Initially, super-saturation of the solution by the neutralization reaction between iron chloride and precipitating agent results in the production of higher rates of mass transfer and nucleation production in the main solution. Then these grains grow in size and already have a size of 9 nm at 20 min to the reaction.

Size of the grains continues to grow based on the mass transfer of iron oxide from supersaturated solution onto the particles already present in the solution. Based on the size of the nanoparticles, the nanoparticles will move toward the walls of the reactor by centripetal forces and will strike the walls of the reactor, will also reduce the size of the nanoparticles. The surface charge of the nanoparticles makes the nanoparticles evenly distributed in the solution, which also results in resistance to agglomeration and coalescence of the nanoparticles resulting in the smaller size of particles. Furthermore, all the nanoparticles are spherical with no sharp edges. This is advantages in the application of these nanoparticles into different forms.

Conclusions

Iron oxide nanoparticles have been prepared via coprecipitation method using precursor mixture of iron (II) chloride and Iron (III) chloride. The nanoparticles are produced in good yield with high impurity and give the reaction rate value of $7.5 \times 10^{-4} \text{ mol min}^{-1}$ with the rate constant of $2.074 \times 10^{-4} \text{ mol}^{-2}\text{min}^{-1}$. The XRD results supported by Raman spectroscopy suggests the formation of the significant portion of maghemite at the early stage of reaction while this maghemite converts to magnetite as reaction proceeds and increase selectivity of magnetite nanoparticles to 98.2%. Furthermore, it is found that Zeta potential of these nanoparticles is -41 at the end of the reaction which

suggests that the nanoparticles are stable and can be used for dispersion of these nanoparticles in different solutions. The surface charge also results in significant resistance toward aggregation and coalesce of nanoparticles. TEM analysis shows that the structure of these nanoparticles are spherical and giving a porous texture. It is believed that these impurity free magnetic nanoparticles with round and the porous surface can be used as an additive in different polymeric materials for its superior magnetic and mechanical properties.

Funding

This work was supported by the University of Malaya through PROTOTYPE DEVELOPMENT RESEARCH GRANT SCHEME (PRGS) [Grant (No. PR005-2014A)].

ORCID

Rizwan Nasir  <http://orcid.org/0000-0001-6618-3231>

References

- [1] Cornell, R.M.; Schwertmann, U. (2003) *The Iron Oxides: Structure, Properties, Reactions, Occurrences and Uses, 2nd, Completely Revised and Extended Edition*, Wiley.
- [2] Mohapatra, M.; Anand, S. (2010) Synthesis and applications of nano-structured iron oxides/hydroxides – a review. *International Journal Engineering Science and Technology*, 2: 127–146.
- [3] Astanina, K.; Simon, Y.; Cavelius, C.; Petry, S.; Kraegeloh, A.; Kiemer, A.K. (2014) Superparamagnetic iron oxide nanoparticles impair endothelial integrity and inhibit nitric oxide production. *Acta Biomaterialia*, 10: 4896–4911. doi: 10.1016/j.actbio.2014.07.027.
- [4] Jha, D.K.; Shameem, M.; Patel, A.B.; Kostka, A.; Schneider, P.; Erbe, A.; Deb, P. (2013) Simple synthesis of superparamagnetic magnetite nanoparticles as

- highly efficient contrast agent. *Materials Letters*, 95: 186–189. doi: [10.1016/j.matlet.2012.12.096](https://doi.org/10.1016/j.matlet.2012.12.096).
- [5] Unni, M.; Uhl, A.M.; Savliwala, S.; Savitzky, B.H.; Dhavalikar, R.; Garraud, N.; Arnold, D.P.; Kourkoutis, L.F.; Andrew, J.S.; Rinaldi, C. (2017) Thermal decomposition synthesis of iron oxide nanoparticles with diminished magnetic dead layer by controlled addition of oxygen. *ACS Nano*, 11 (2): 2284–2303. doi: [10.1021/acsnano.7b00609](https://doi.org/10.1021/acsnano.7b00609).
- [6] Kong, L.; Gan, X.; Bin Ahmad, A.L.; Hamed, B.H.; Evarts, E.R.; Ooi, B.; Lim, J. (2012) Design and synthesis of magnetic nanoparticles augmented microcapsule with catalytic and magnetic bifunctionalities for dye removal. *Chemical Engineering Journal and the Biochemical Engineering Journal*, 197: 350–358.
- [7] Pellico, J.; Ruiz-Cabello, J.; Saiz-Alía, M.; Del Rosario, G.; Caja, S.; Montoya, M.; Fernández de Manuel, L.; Morales, M.P.; Gutiérrez, L.; Galiana, B.; Enríquez, J.A.; Herranz, F. (2016) Fast synthesis and bioconjugation of ⁶⁸Ga core-doped extremely small iron oxide nanoparticles for PET/MR imaging. *Contrast Media Molecular Imaging*, 11 (3): 203–210. doi: [10.1002/cmimi.1681](https://doi.org/10.1002/cmimi.1681).
- [8] Zhang, X.; Niu, H.; Pan, Y.; Shi, Y.; Cai, Y. (2011) Modifying the surface of Fe₃O₄/SiO₂ magnetic nanoparticles with C18/NH₂ mixed group to get an efficient sorbent for anionic organic pollutants. *Journal of Colloid and Interface Science*, 362: 107–112. doi: [10.1016/j.jcis.2011.06.032](https://doi.org/10.1016/j.jcis.2011.06.032).
- [9] Bennett, R.A.; Etman, H.A.; Hicks, H.; Richards, L.; Wu, C.; Castell, M.R.; Dhessi, S.S.; Maccherozzi, F. (2018) Magnetic iron oxide nanowires formed by reactive dewetting. *Nano Letters*, 18 (4): 2365–2372. doi: [10.1021/acs.nanolett.7b05310](https://doi.org/10.1021/acs.nanolett.7b05310).
- [10] Alizadeh, T.; Jahani, R. (2015) A new strategy for low temperature gas sensing by nano-sized metal oxides: development a new nerve agent simulant sensor. *Materials Chemistry and Physics*, 168: 180–186. doi: [10.1016/j.matchemphys.2015.11.019](https://doi.org/10.1016/j.matchemphys.2015.11.019).
- [11] Saritas, S.; Kundakci, M.; Coban, O.; Tuzemen, S.; Yildirim, M. (2018) Ni: Fe₂O₃, Mg: Fe₂O₃ and Fe₂O₃ thin films gas sensor application. *Physics B Condensed Matter*, 541: 14–18. doi: [10.1016/j.physb.2018.04.028](https://doi.org/10.1016/j.physb.2018.04.028).
- [12] Wajjarean, N.; MacKenzie, K.J.D.; Asavapisit, S.; Piyaphanuwat, R.; Jameson, G.N.L. (2017) Synthesis and properties of geopolymers based on water treatment residue and their immobilization of some heavy metals. *Journal of Materials Science*. doi: [10.1007/s10853-017-0970-4](https://doi.org/10.1007/s10853-017-0970-4).
- [13] Liu, G.; Cai, M.; Wang, X.; Zhou, F.; Liu, W. (2016) Magnetite-Loaded Thermosensitive Nanogels for Bioinspired Lubrication and Multimodal Friction Control. *ACS Macro Letters*, 5: 144–148. doi: [10.1021/acsmacrolett.5b00860](https://doi.org/10.1021/acsmacrolett.5b00860).
- [14] Fernández-Ibáñez, M.Á. (2014) Ligands control reactivity and selectivity in palladium-catalyzed functionalization of unactivated Csp³ H bonds. *Chemical Catalysis Catalytic Chemistry*, 6: 2188–2190.
- [15] De Martino, M.T.; Abdelmohsen, L.K.E.A.; Rutjes, F.P. J.T.; van Hest, J.C.M. (2018) Nanoreactors for green catalysis. *Beilstein Journal of Organic Chemistry*, 14: 716–733. doi: [10.3762/bjoc.14.61](https://doi.org/10.3762/bjoc.14.61).
- [16] Mascolo, M.C.; Pei, Y.; Ring, T.A. (2013) Room temperature co-precipitation synthesis of magnetite nanoparticles in a large pH window with different bases. *Materials (Basel)*, 6: 5549–5567. doi: [10.3390/ma6125549](https://doi.org/10.3390/ma6125549).
- [17] Gatelyte, A.; Jasaitis, D.; Beganskiene, A.; Kareiva, A. (2011) Sol-gel synthesis and characterization of selected transition metal nano-ferrites. *Medziagotyra*, 17 (3):302–307.
- [18] Sinha, M.K.; Sahu, S.K.; Meshram, P.; Prasad, L.B.; Pandey, B.D. (2015) Low temperature hydrothermal synthesis and characterization of iron oxide powders of diverse morphologies from spent pickle liquor. *Powder Technology*. doi: [10.1016/j.powtec.2015.02.006](https://doi.org/10.1016/j.powtec.2015.02.006).
- [19] Sahoo, S.K.; Agarwal, K.; Singh, A.K.; Polke, B.G.; Raha, K.C. (2010) Characterisation of γ- and α-Fe₂O₃ nano powders synthesised by emulsion precipitation-calcination route and rheological behaviour of α-Fe₂O₃. *International Journal of Engineering, Science and Technology*, 2 (8): 118–126.
- [20] Sachdev, S.; Maugi, R.; Kirk, C.; Zhou, Z.; Christie, S.D. R.; Platt, M. (2017) Synthesis and assembly of gold and iron oxide particles within an emulsion droplet; facile production of core@shell particles. *Colloids and Interface Science Communications*, 16: 14–18. doi: [10.1016/j.colcom.2016.12.005](https://doi.org/10.1016/j.colcom.2016.12.005).
- [21] Rizzuti, A.; Dassisti, M.; Mastrorilli, P.; Sportelli, M. C.; Cioffi, N.; Picca, R.A.; Agostinelli, E.; Varvaro, G.; Caliendo, R. (2015) Shape-control by microwave-assisted hydrothermal method for the synthesis of magnetite nanoparticles using organic additives. *Journal of Nanoparticle Research*, 17. doi: [10.1007/s11051-015-3213-0](https://doi.org/10.1007/s11051-015-3213-0).
- [22] Thanh, N.T.K.; Maclean, N.; Mahiddine, S. (2014) Mechanisms of nucleation and growth of nanoparticles in solution, *Chemical Reviews*. 114 (15): 7610–7630
- [23] Alexandrov, D.V.; Ivanov, A.A.; Alexandrova, I.V. (2018) The influence of Brownian coagulation on the particle-size distribution function in supercooled melts and supersaturated solutions. *Journal of Physics A: Mathematical and Theoretical*, 52: 15101. doi: [10.1088/1751-8121/aaefdc](https://doi.org/10.1088/1751-8121/aaefdc).
- [24] Okada, K.; Akagi, Y.; Kogure, M.; Yoshioka, N. (1990) Effect of surface charges of bubbles and fine particles on air flotation process. *The Canadian Journal of Chemical Engineering*, 68 (3): 393–399. doi: [10.1002/cjce.5450680307](https://doi.org/10.1002/cjce.5450680307).
- [25] Jeldres, R.I.; Fawell, P.D.; Florio, B.J. (2018) Population balance modelling to describe the particle aggregation process: A review. *Powder Technology*, 326: 190–207. doi: [10.1016/j.powtec.2017.12.033](https://doi.org/10.1016/j.powtec.2017.12.033).
- [26] Wei, D.; Dave, R.; Pfeffer, R. (2002) Mixing and characterization of nanosized powders: an assessment of different techniques. *Journal of Nanoparticle Research*, 4: 21–41. doi: [10.1023/A:1020184524538](https://doi.org/10.1023/A:1020184524538).
- [27] Tai, M.F.; Lai, C.W.; Hamid, S.B.A.; Suppiah, D.D.; Lau, K.S.; Yehya, W.A.; Julkapli, N.M.; Lee, W.H.; Lim, Y.S. (2014) Facile synthesis of magnetite iron oxide nanoparticles via precipitation method at different reaction temperatures. *Innovations Materials Research Innovations*, 18: S6-470-S6-473.
- [28] Mahdavi, M.; Bin Ahmad, M.; Haron, M.J.; Namvar, F.; Nadi, B.; Rahman, M.Z.A.; Amin, J. (2013) Synthesis, surface modification and characterisation of biocompatible magnetic iron oxide nanoparticles for biomedical applications. *Molecules*, 18: 7533–7548. doi: [10.3390/molecules18077533](https://doi.org/10.3390/molecules18077533).

- [29] Ardizzone, S.; Formaro, L. (1983) Temperature induced phase transformation of metastable $\text{Fe}(\text{OH})_3$ in the presence of ferrous ions. *Materials Chemistry and Physics*, 8: 125–133. doi: [10.1016/0254-0584\(83\)90046-9](https://doi.org/10.1016/0254-0584(83)90046-9).
- [30] Kim, W.; Suh, C.-Y.; Cho, S.-W.; Roh, K.-M.; Kwon, H.; Song, K.; Shon, I.J. (2012) A new method for the identification and quantification of magnetite–maghemite mixture using conventional X-ray diffraction technique. *Talanta*, 94: 348–352. doi: [10.1016/j.talanta.2012.03.001](https://doi.org/10.1016/j.talanta.2012.03.001).
- [31] Bonsack, J.P. (1989) Process for partial oxidation of FeCl_2 to FeCl_3 . *Google Patents*
- [32] Baumgartner, J.; Dey, A.; Bomans, P.H.H.; Le Coadou, C.; Fratzl, P.; Sommerdijk, N.A.J.M.; Faivre, D. (2013) Nucleation and growth of magnetite from solution. *Nature Materials*, 12: 310–314. doi: [10.1038/nmat3558](https://doi.org/10.1038/nmat3558).
- [33] Saafan, S.A.; Meaz, T.M.; El-Ghazzawy, E.H. (2011) Study of DC conductivity and relative magnetic permeability of nanoparticle $\text{NiZnFe}_2\text{O}_4/\text{PPy}$ composites. *Journal of Magnetism and Magnetic Materials*, 323: 1517–1524. doi: [10.1016/j.jmmm.2011.01.010](https://doi.org/10.1016/j.jmmm.2011.01.010).
- [34] Subramanian, M.; Miaskowski, A.; Jenkins, S.I.; Lim, J.; Dobson, J. (2018) Remote manipulation of magnetic nanoparticles using magnetic field gradient to promote cancer cell death. *BioRxiv*, 317115.
- [35] Shanmugavelayutham, G.; Saravanan, P.; Balasubramanian, C. (2018) Rapid synthesis of nano-magnetite by thermal plasma route and its magnetic properties. AU - Koushika, E. M *Processes Materials and Manufacturing Processes*, 33: 1701–1707. doi: [10.1080/10426914.2018.1453163](https://doi.org/10.1080/10426914.2018.1453163).
- [36] Men, H.-F.; Liu, H.-Q.; Zhang, Z.-L.; Huang, J.; Zhang, J.; Zhai, -Y.-Y.; Li, L. (2012) Synthesis, properties and application research of atrazine $\text{Fe}_3\text{O}_4@ \text{SiO}_2$ magnetic molecularly imprinted polymer, *Environ. Science and Pollution Research*, 19: 2271–2280. doi: [10.1007/s11356-011-0732-9](https://doi.org/10.1007/s11356-011-0732-9).
- [37] Bini, R.A.; Marques, R.F.C.; Santos, F.J.; Chaker, J.A.; Jafellici, M. (2012) Synthesis and functionalization of magnetite nanoparticles with different amino-functional alkoxy silanes. *Journal of Magnetism and Magnetic Materials*, 324: 534–539. doi: [10.1016/j.jmmm.2011.08.035](https://doi.org/10.1016/j.jmmm.2011.08.035).
- [38] Domaschke, M.; Schmidt, M.; Peukert, W. (2018) A model for the particle mass yield in the aerosol synthesis of ultrafine monometallic nanoparticles by spark ablation. *Journal of Aerosol Science*, 126: 133–142. doi: [10.1016/j.jaerosci.2018.09.004](https://doi.org/10.1016/j.jaerosci.2018.09.004).
- [39] Hansen, T.W.; DeLaRiva, A.T.; Challa, S.R.; Datye, A. K. (2013) Sintering of catalytic nanoparticles: particle migration or ostwald ripening. *Accounts of Chemical Research*, 46 (1): 1720–1730. doi: [10.1021/ar3002427](https://doi.org/10.1021/ar3002427).
- [40] Kong, C.-P.; Peters, E.A.J.F.; de With, G.; Zhang, H.-X. (2013) Molecular dynamics simulation of a DOPA/ST monolayer on the Au(111) surface. *Physical Chemistry Chemical Physics*, 15: 15426–15433. doi: [10.1039/c3cp51973b](https://doi.org/10.1039/c3cp51973b).